Monthly Notices of the ROYAL ASTRONOMICAL SOCIETY

MNRAS **487,** 1149–1159 (2019) doi:10.1093/mnras/stz1284
Advance Access publication 2019 May 11

A low-mass triple system with a wide L/T transition brown dwarf component: NLTT 51469AB/SDSS 2131−0119

B. Gauza [1,2★†] V. J. S. Béjar,[2,3] A. Pérez-Garrido,[4] N. Lodieu,[2,3] R. Rebolo,[2,3,5] M. R. Zapatero Osorio,[6] B. Pantoja,[1] S. Velasco [2,3] and J. S. Jenkins[1]

[1]*Departamento de Astronomía, Universidad de Chile, Camino El Observatorio 1515, Las Condes, Santiago, Chile*
[2]*Instituto de Astrofísica de Canarias (IAC), Calle Vía Láctea s/n, E-38200 La Laguna, Tenerife, Spain*
[3]*Departamento de Astrofísica, Universidad de La Laguna (ULL), E-38206 La Laguna, Tenerife, Spain*
[4]*Universidad Politécnica de Cartagena, Campus Muralla del Mar, Cartagena, Murcia E-30202, Spain*
[5]*Consejo Superior de Investigaciones Científicas, CSIC, Serrano, 117, E-28006 Madrid, Spain*
[6]*Centro de Astrobiología (CSIC-INTA), Ctra. Ajalvir km 4, E-28850 Torrejón de Ardoz, Madrid, Spain*

Accepted 2019 April 30. Received 2019 March 21; in original form 2018 October 4

ABSTRACT

We demonstrate that the previously identified L/T transition brown dwarf SDSS J213154.43−011939.3 (SDSS 2131−0119) is a widely separated (82.″3, ∼3830 au) common proper motion companion to the low-mass star NLTT 51469, which we reveal to be a close binary itself, separated by 0.″64 ± 0.″01 (∼30 au). We find the proper motion of SDSS 2131−0119 of $\mu_\alpha \cos\delta = -100 \pm 20$ mas yr^{-1} and $\mu_\delta = -230 \pm 20$ mas yr^{-1} consistent with the proper motion of the primary provided by *Gaia* DR2: $\mu_\alpha \cos\delta = -95.49 \pm 0.96$ mas yr^{-1} and $\mu_\delta = -239.38 \pm 0.96$ mas yr^{-1}. Based on optical and near-infrared spectroscopy, we classify the primary NLTT 51469A as an M3 ± 1 dwarf, estimate photometrically the spectral type of its close companion NLTT 51469B at ∼M6, and confirm the spectral type of the brown dwarf to be L9 ± 1. Using radial velocity, proper motion, and parallax, we derived the *UVW* Galactic space velocities of NLTT 51469A, showing that the system does not belong to any known young stellar moving group. The high *V*, *W* velocities, lack of a 670.8 nm Li I absorption line, and absence of Hα emission, detected X-rays, or UV excess, indicate that the system is likely a member of the thin disc population and is older than 1 Gyr. For the parallactic distance of 46.6 ± 1.6 pc from *Gaia* DR2, we determined luminosities of $-1.50^{+0.02}_{-0.04}$ and −4.4 ± 0.1 dex of the M3 and L9, respectively. Considering the spectrophotometric estimation, which yields a slightly lower distance of 34^{+10}_{-13} pc, the obtained luminosities are $-1.78^{+0.02}_{-0.04}$ and $-4.7^{+0.3}_{-0.5}$ dex. We also estimated their effective temperatures and masses, and obtained 3410^{+140}_{-210} K and 0.42 ± 0.02 M$_\odot$ for the primary, and 1400–1650 K and 0.05–0.07 M$_\odot$ for the wide companion. For the ∼M6 component, we estimated $T_{\rm eff} = 2850 \pm 200$ K and $m = 0.10^{+0.06}_{-0.01}$ M$_\odot$.

Key words: proper motions – brown dwarfs – stars: individual: NLTT 51469 – stars: low-mass.

1 INTRODUCTION

Brown dwarfs are objects that have insufficient mass to sustain stable nuclear fusion in their interiors. After they are formed they evolve getting fainter and cooler. The emergent spectra of brown dwarfs were found so different from that of the latest type M dwarf stars that the establishment of two new spectral types, L and T (Kirkpatrick et al. 1999; Burgasser et al. 2006a), was indispensable to properly classify them. The L-type class encompasses the least massive stars and most massive brown dwarfs and spans effective temperatures ($T_{\rm eff}$s) of approximately 2500–1300 K (e.g. Kirkpatrick et al. 1999; Kirkpatrick 2005). The T-type class includes solely brown dwarfs with temperatures below ∼1400 K and down to 500–700 K (e.g. Golimowski et al. 2004; Burgasser, Burrows

★ E-mail: bgauza87@gmail.com
† Based on observations made with the Gran Telescopio Canarias (GTC), installed in the Spanish Observatorio del Roque de los Muchachos of the Instituto de Astrofísica de Canarias, in the island of La Palma (program GTC27-13B).

& Kirkpatrick 2006b; Burgasser et al. 2006a; Burningham et al. 2008; Leggett et al. 2009). Most recently, searches using the space-based Wide-field Infrared Survey Explorer (WISE; Wright et al. 2010) data revealed a population of even lower $T_{\rm eff}$ objects from approximately 500–700 K down to about 250 K, which have been classified as Y dwarfs (e.g. Cushing et al. 2011; Kirkpatrick et al. 2012; Luhman 2014; Leggett et al. 2017).

The L to T-type transition undergoes a dramatic change in near-infrared (near-IR) $J - K_{\rm s}$ colour, which becomes bluer by about 2 mag as part of a major change in spectral morphology. This occurs over a narrow range in temperature $\Delta T_{\rm eff} \sim$ 200–300 K (e.g. Golimowski et al. 2004). This dynamic phenomenon is still not entirely reproduced and matched by theoretical models, nevertheless the general description of the L/T transition is thought to be fairly well understood for high-gravity atmospheres. It is physically characterized by the breakup and clearing of the condensate clouds and a sudden sedimentation of condensed species below the photosphere when the local temperature is $\lesssim$1500 K, and by the appearance of methane absorption in the 1.0–2.5 μm region (Allard et al. 1997, 2001; Chabrier et al. 2000; Ackerman & Marley 2001; Burrows, Sudarsky & Hubeny 2006; Saumon & Marley 2008).

Since the discoveries of the first unambiguous brown dwarfs in the mid 1990s (Nakajima et al. 1995; Rebolo, Zapatero Osorio & Martín 1995), large-area imaging surveys in optical and near-IR wavelengths like, among others, DENIS (Epchtein et al. 1994), 2MASS (Skrutskie et al. 2006), Sloan Digital Sky Survey (SDSS; York et al. 2000; Abazajian et al. 2003), and more recently UKIDSS (Lawrence et al. 2007), *WISE* (Wright et al. 2010), and Pan-STARRS (Kaiser et al. 2002) enabled significant growth in the population of known brown dwarfs with the current number being around 2000 objects (Delfosse et al. 1997; Kirkpatrick 2005; Kirkpatrick et al. 2011; Scholz et al. 2012; Deacon et al. 2014; Robert et al. 2016; Smart et al. 2017). However, a great majority of these are single objects and only a small fraction are found to be components in binary or multiple systems (e.g. Faherty et al. 2010; Deacon et al. 2014; Baron et al. 2015; Scholz 2016).

Ultracool companions to stars are of interest because both components share the same age, metallicity, and distance, which are easier to determine for the brighter primary. Substellar objects with well-constrained age and metallicity are valuable reference points for calibrating evolutionary and atmospheric models (e.g. Pinfield et al. 2006; Faherty et al. 2010; Jenkins et al. 2012; Gomes et al. 2013; Marocco et al. 2017). Widely separated substellar companions are particularly useful for characterization because they can be directly observed using seeing-limited instruments.

In this paper, we present a nearby, common proper motion triple system identified in our search for ultracool companions to stars using the VISTA Hemisphere Survey (VHS) data. We describe the search and identification methods in Section 2. Section 3 contains the description of follow-up observations aimed at confirming the companionship and characterization of the objects. Next, we determine the spectral types of the components in Section 4 and demonstrate the binarity of the NLTT 51469 star in Section 5. In Section 6, we compare the distance measured by *Gaia* to the spectrophotometric distance obtained for the primary and the L9 companion. Section 7 contains a discussion on the probability of chance alignment of the two wide components. In Section 8, we determine the physical properties of the objects, including radial velocity, galactic kinematics, and constraint on the age of the system, luminosities, masses, and temperatures of the individual components. Conclusions and future prospects are presented in Section 9.

2 SEARCH AND IDENTIFICATION

The VHS (Emerson et al. 2004) is an ongoing imaging survey for which one of the main goals is the detection of very low mass stars and substellar objects. The VHS will map the entire Southern hemisphere of the sky (∼20 000 deg^2), with the exception of the areas within the VISTA Kilo-Degree Infrared Galaxy Survey (VIKING) and the Variables in the Via Lactea (VVV) survey. Observations covering an area of 10 000 deg^2 are carried out in two near-IR bands, J and $K_{\rm s}$, 5000 deg^2 in $JHK_{\rm s}$ and another 5000 deg^2 in $YJHK_{\rm s}$, reaching a median 5σ point source detection limit of $J = 20.2$ and $K_{\rm s} = 18.1$ mag (McMahon et al. 2013). The VHS catalogue provides astrometry and photometry in the J, $K_{\rm s}$ bands, and Y, H bands when available. The VISTA photometric system is calibrated using the magnitudes of colour-selected 2MASS stars converted on to the VISTA system using colour equations, including terms to account for interstellar reddening.[1] Photometric calibrations are determined to an accuracy of 1–2 per cent. The astrometric solution for VHS observations is computed by the automatic pipeline of the survey, using point sources from the 2MASS catalogue. The world coordinate system of VISTA images is calibrated to 0.1–0.2 arcsec accuracy.

As of the early data releases from VHS prior to 2013 March, which covered about 8500 deg^2, we built a catalogue of high proper motion objects in the Southern hemisphere, with motions greater than 0.15–0.20 arcsec per year. We combined VHS catalogue measurements (astrometry and $YJHK$ photometry) with 2MASS point source catalogue measurements (as a reference epoch) to identify moving objects in the sky areas overlapping with VHS. The time baseline between the two surveys (>10 yr) allows us to measure proper motions with a precision of 10 mas yr^{-1} or better. Our search was restricted to sources with $J_{\rm 2MASS} \leq 17.5$ mag, and fainter than $J_{\rm VHS} = 11$ mag to exclude objects affected by saturation from the VHS data base. We also cross-matched VHS sources with WISE All-Sky and USNO-B1.0 catalogues to get mid-infrared and optical photometry information and to filter out contaminants based on mid-infrared and optical constraints where available.

In the cross-correlation of VHS and 2MASS catalogues, we have found 50 382 objects with a $J = 11$–17.5 mag range and proper motions of $\mu \gtrsim 150$ mas yr^{-1} taking into account the baseline of 10–12 yr between these two surveys. Most of these high proper motion objects are relatively nearby M dwarfs with estimated photometric distances within 100 pc. The general catalogue is currently being developed and prepared for publication (A. Pérez-Garrido et al., in preparation). Among this list, we have searched for objects co-moving with stars from the revised version of the New Luyten Catalogue of Stars with Proper Motions Larger than Two Tenths of an Arcsecond (NLTT; Gould & Salim 2003; Salim & Gould 2003). We required proper motions to be consistent within 50 mas yr^{-1} in both right ascension and declination to identify proper motion pairs. This corresponds to a factor of 2.5–3 times larger than the quoted 1 σ astrometric error of the surveys, which improves the scope for identifying moving objects fainter than the 2MASS completeness

[1] http://casu.ast.cam.ac.uk/surveys-projects/vista/technical/photometric-properties

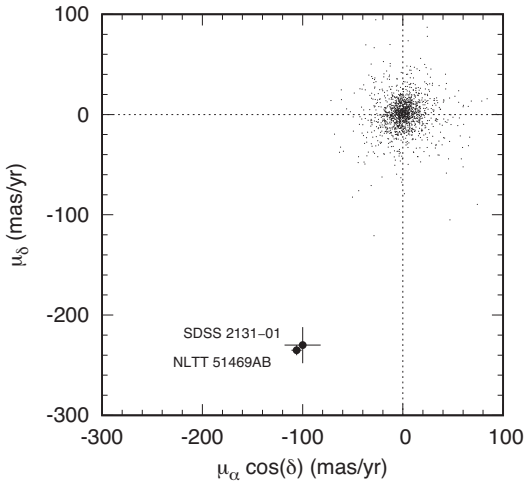

Figure 1. Proper motion vector-point diagram for NLTT 51469 and its companion. All correlated objects within 20 arcmin from the primary with $J < 17.5$ mag are plotted as black dots, while the two components of the common proper motion pair are plotted with larger points and labelled. Error bars correspond to the astrometric rms of stars with similar brightness as of the components.

limits. The cross-match was limited to angular separations of a 20 arcmin radius.

From the more than a hundred potential binaries and multiples, we build a sample of candidate systems containing one or more components with near- and mid-IR photometric colours consistent with mid-M and later spectral types ($J - K_s > 0.8$, $J - H > 0.5$, $J - W2 > 1.5$, $W1 - W2 > 0.5$). Next, we verified each selected system, by checking for the consistency in distance modulus of its candidate components, estimated roughly from the apparent J-band brightness and the expected spectral type based on photometric colours. The colour-spectral type and colour-absolute magnitude relations were adopted from Chiu et al. (2006), Kirkpatrick et al. (2011), and Dupuy & Liu (2012).

One of the identified pairs was the star NLTT 51469 and the brown dwarf SDSS J213154.43−011939.3 with on-sky separation of 82.3 arcsec. In the VHS-2MASS cross-match, we obtained proper motions of $\mu_\alpha \cos\delta$, $\mu_\delta = -82 \pm 16$, -229 ± 18 and -60 ± 19, -270 ± 20 mas yr^{-1}, for the primary and companion, respectively. The values are consistent within 50 mas yr^{-1} as required, but the differences are around 1σ error. We note that the centroid positions are likely unreliable, because of the brightness range of the surveys. On the one hand, the primary is out of the linear range of the VHS and on the other hand, the secondary is close to detection limit in 2MASS. Therefore, we employed also the SDSS astrometry, and obtained more precise proper motions by combining 2MASS and SDSS measurements for the M3 star, and VHS and SDSS measurements for the L9 brown dwarf. The resulting values are $\mu_\alpha \cos\delta$, $\mu_\delta = -106 \pm 8$, -235 ± 8 mas yr^{-1} for the M3 and -100 ± 15, -230 ± 15 mas yr^{-1} for the L9. This is also in good agreement with the *Gaia* Data Release 2 measurement for the primary, which gives $\mu_\alpha \cos\delta$, $\mu_\delta = -95.49 \pm 0.96$, -239.38 ± 0.96 mas yr^{-1} (Gaia Collaboration 2016, 2018). To within the quoted uncertainties, both objects share the same proper motion, which is shown in Figure 1. These proper motions differ significantly ($>10\sigma$) from the population of background field stars (with $J < 17.5$ mag and within 20 arcmin) also shown in the figure. The J -band finding chart for the system is displayed in Figure 2.

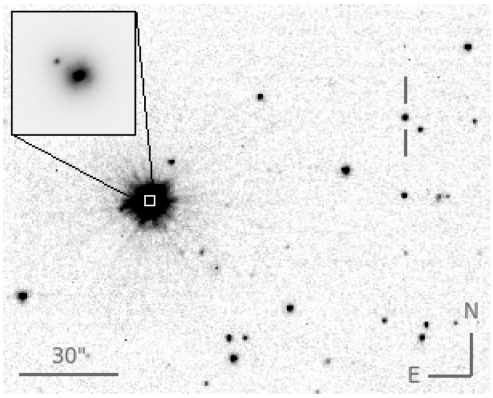

Figure 2. VISTA J-band image of the NLTT 51469/SDSS 2131−0119 system, with the location of the brown dwarf component marked with two vertical lines. The field shown is 3 arcmin × 2.5 arcmin and oriented North-up and East to the left. The zoomed-in region showing the central binary is the 3 arcsec × 3 arcsec MagAO/Clio2 image.

3 FOLLOW-UP OBSERVATIONS AND DATA REDUCTION

3.1 Near-IR spectroscopy

We obtained low-resolution near-IR spectroscopy of the primary NLTT 51469A using the Son of ISAAC (SofI) spectro-imager installed on the NTT on 2013 November 16 [programme ID: 092.C-0874(B), PI: Gauza]. SofI is equipped with a Hawaii HgCdTe 1024 × 1024 array with 18.5 μm pixels. We used the large-field mode, offering a field of view of 4.9 × 4.9 arcmin with a 0.288 arcsec pixel scale, and blue (950–1640 nm) and red (1530–2520 nm) grisms combined with a slit of 1 arcsec oriented to the parallactic angle. This configuration provides a resolving power of $R \sim 550$. We used single integrations of 60 and 120 s for blue and red grisms, respectively, repeated in an ABBA pattern for both the configurations to remove the sky contribution. To correct for telluric absorption features, we observed an early-type hot star with the same configuration (HD 13936; $J = 6.46$ mag; A0V; van Leeuwen 2007) shortly after NLTT 51469A but at a lower airmass (1.2 versus 2.4). The sky conditions during the observations were clear with a seeing around 1 arcsec. During the afternoon preceding the observations, we acquired standard calibration frames for data reduction, including bias, spectral flats, and Xenon arcs.

We used the ESO SofI pipeline recipes version 1.5.5 within the GASGANO tool to reduce the raw data and to align and combine the dispersed images from the four ABBA positions along the slit to obtain images of the 2D spectra. We then extracted the spectra using standard routines under the APALL task in IRAF and wavelength calibrated it via Xenon arc lines. The dispersion solution had an rms of 0.54 and 0.62 Å for the blue and red parts of the spectrum, respectively, and the resolution of the spectra was 24 Å ($R \sim 530$) and 35 Å ($R \sim 580$) in the blue and red arms, respectively. We corrected for telluric lines, dividing the spectra by the A0V standard HD 13936 and multiplying by a blackbody of a corresponding effective temperature of 9700 K.

3.2 Optical spectroscopy

We performed long-slit, low-resolution optical spectroscopy of NLTT 51469 and its wide companion using the OSIRIS instrument (Optical System for Imaging and low-intermediate Resolution Integrated Spectroscopy; Cepa 2010) at the Gran Telescopio de Canarias (GTC) telescope located on the Observatorio del Roque de los Muchachos (island of La Palma, Spain). OSIRIS is equipped with two 2048 × 4096 Marconi CCD42-82 detectors, which provides a field of view of approximately 7×7 arcmin^2 with an unbinned pixel scale of 0.125 arcsec.

We observed both objects using an R300R grating with a slit width of 2.5 arcsec and 2×2 binning, which allowed us to measure the general spectral energy distribution at a resolution of 87Å ($R \sim 76$), covering the 0.5–1.0 μm range. Observations were acquired on 2013 October 26 as part of the GTC27-13B programme (PI: N. Lodieu). Single exposures of 15 and 600 s were obtained for the primary and secondary, respectively. Bias frames, continuum lamp flat-fields, and Xenon, Neon, and Argon arcs were obtained during the afternoon preceding the observations. The spectrophotometric standard star G158−100 (Filippenko & Greenstein 1984; Oke 1990) was observed on the same night as the scientific target, first using the same spectroscopic set-up as for the target, and then also with a broad z-band filter to correct for second-order contamination beyond 9200 Å (see procedure in Zapatero Osorio et al. 2014).

The OSIRIS data were reduced with standard procedures using routines within IRAF. The raw spectra were bias-corrected, trimmed, and divided by a normalized continuum lamp flat-field. From the 2D images, we extracted the spectra using the APALL routine and calibrated in wavelength with the lines from combined XeNeAr arc lamps. The correction for instrumental response was applied using a response function generated from the spectrophotometric standard star.

To look for spectral signatures of age like, e.g. the lithium Li I line at 670.8 nm or Hα emission at 656.3 nm and also to obtain additional measurement of radial velocity of the primary star, we acquired intermediate-resolution ($R \sim 5000$) optical spectroscopy of NLTT 51469 using the Fibre-fed RObotic Dual-beam Optical Spectrograph (FRODOSpec; Morales-Rueda et al. 2004) on the robotic Liverpool Telescope (LT; Steele et al. 2004) in La Palma. The FRODOSpec is a 12×12 fibre integral-field unit spectrograph for the LT, designed mainly to study point sources. Each fibre covers a field of view on sky of ∼0.83 arcsec × 0.83 arcsec, corresponding to a total field of view of approximately 10 arcsec × 10 arcsec (Morales-Rueda et al. 2004; Barnsley, Smith & Steele 2012). It uses a dichroic beam splitter to separate the incident light at around 5750 Å, into the blue and red arms, covering in the high-resolution mode 3900–5100 and 5900–8000 Å, respectively.

We used the Volume Phase Holographic (VPH) grating available on the instrument, which provides higher resolution ($R \sim 5300$ in red arm) than the conventional diffraction grating. Observations of NLTT 51469 were performed on 2016 July 24. Two individual exposures of 600 s integrations were collected. A radial velocity standard star GJ 873 was observed with the same instrumental set-up and 30 s integrations on 2016 August 20. The Xenon arcs and Tungsten lamp exposures were acquired prior to each target. Raw FRODOSpec data were reduced by two sequentially invoked automatic pipelines. The first one, known as the L1, processes the CCD images performing bias subtraction, overscan trimming, and flat-fielding. The second one (L2) performs the processing appropriate to integral-field spectra reduction. Details of the processing steps of the two pipelines are described in Barnsley et al. (2012).

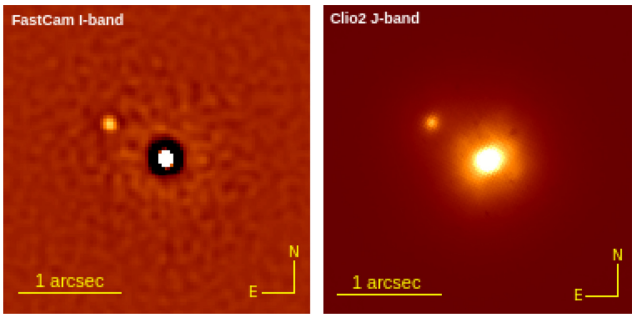

Figure 3. Resolved images of the central binary NLTT 51469AB. *Left:* The NOT/FastCam *I*-band image after lucky imaging processing and the wavelet filtering. *Right:* The MagAO/Clio2 *J*-band image. The companion is detected at 0.63 arcsec separation and position angle of ∼57 deg. The displayed field of view is 3 arcsec × 3arcsec.

The reduced data products contain a snapshot of the data taken at key stages in the reduction process, including the final sky-subtracted and wavelength-calibrated 1D spectra. No correction of the instrumental response was applied.

Since the K I line at 766.5 nm is strongly affected by telluric lines, we applied a telluric correction to measure the pEW of these lines. For this purpose, we divided the spectrum of the target by the spectrum of a hot, early-type star (BD+28 4211, sdO) observed on the same night. The spectrum of telluric star was first normalized in the whole spectral range except parts affected by telluric absorption. We only used this telluric-corrected spectrum for this purpose, because the S/N of the telluric star spectrum was poor and introduced more noise to the rest of the spectrum of our target.

3.3 NOT/FastCam lucky imaging

On 2016 November 16, we collected 5000 individual frames of NLTT 51469 in the *I* band using the lucky imaging FastCam instrument (Oscoz et al. 2008) at the 2.4 m Nordic Optical Telescope (NOT) at the Observatorio del Roque de Los Muchcachos in La Palma, with a 30 ms exposure time for each frame. FastCam is an optical imager with a low-noise EMCCD camera, which allows us to obtain speckle-featuring not saturated images at a high frame rate. In order to construct a high spatial resolution, diffraction-limited, long-exposure image, the individual frames were bias subtracted, aligned, and co-added using our own lucky imaging algorithm (Labadie et al. 2011; Velasco et al. 2016). Fig. 3 presents the high-resolution image constructed by co-addition of the best percentage of the images using the lucky imaging and shift-and-add method and processed with the wavelet-filtering algorithm. Owing to the atmospheric conditions of the night, the selection of 10 per cent of the individual frames was found to be the best solution to produce a deep and diffraction-limited image of the target, resulting in a total integration time of 15 s. To calibrate the plate scale and orientation, we used observations of the M15 globular cluster core performed on the same night compared against the *HST* WFPC2 catalogue of M15 (van der Marel et al. 2002).

3.4 Clay/MagAO imaging

We observed NLTT 51469 using the Magellan Clay telescope at Las Campanas Observatory in Chile on the night of 2018 May 2. Observations were performed in the *J* band using the infrared

camera Clio-2 in the narrow mode, which provides a field of view of 16 arcsec × 8 arcsec (Morzinski et al. 2015). We nodded in an ABBA pattern to subtract the background and obtained five frames of 10 s integration at each nod position. In the same manner, we acquired shallow, unsaturated images with shorter, 0.5 s individual integrations for the photometry. Shortly after the science target, we observed the binary star 70 Oph that has an accurately determined orbit (Pourbaix 2000) for the calibration of the pixel scale and orientation.

We reduced the raw data cubes using PYRAF routines, which included subtraction of the proper nod pairs to remove the sky contribution, registering, aligning, and median stacking of the individual frames. From the obtained image of 70 Oph, we calculated the plate scale of 15.523 ± 0.254 mas pixel^{-1} and the NORTHClio angle of -1.78 ± 0.40 deg. The NORTHClio angle is then used to find the derotation angle needed to get the North-up and East-left orientation. These values are consistent with the nominal values of 15.846 ± 0.064 mas pixel^{-1} and NORTHClio $= -1.797 \pm 0.34$ deg provided in Morzinski et al. (2015). A 3 × 3 arcsec cut-off of the final derotated image of the pair is presented in Fig. 3.

3.5 VLT/NACO imaging

We also acquired near-IR J, H, K_s images of the primary using the NACO instrument, short for the Nasmyth Adaptive Optics System (NAOS; Rousset et al. 2003) of the VLT-UT1, coupled to the CONICA high-contrast infrared camera (Lenzen et al. 1998). Observations were completed on 2018 October 24 [programme ID 0102.C-0899(A), PI Gauza], at an average airmass of 1.1 and with thin cirrus clouds. We used the infrared wavefront sensor with the N90C10 dichroic, and our target star as a natural guide star. We chose high-sensitivity mode of CONICA with the FowlerNsamp read-out and the S13 objective that provides a 14 arcsec × 14 arcsec field of view and the smallest available pixel scale of 13.26 ± 0.03 mas pixel^{-1} (Masciadri et al. 2003). Individual exposures of 60 and 20 s were taken in a 5 and 9 position jittering pattern for the J and H, K_s filters, respectively, for a proper sky background subtraction. In the same observing block, with the same set-up and observing technique we also obtained K_s-band images of a known binary star WDS 20204+0118 (Mason et al. 2001) for pixel scale and orientation calibration.

Raw images were processed using the ESO NACO pipeline kit version 4.4.6, run within the GASGANO software tool, version 2.4.8. This included the dark and flat-field corrections, sky subtraction, alignment of individual frames, and stacking of each frameset. Astrometric and photometric measurements obtained from the final reduced JHK_s images are described in Section 5.

4 SPECTRAL CLASSIFICATION

We based the spectral type determination for the two components of this system on the low-resolution spectra, optical and near-IR for the primary, and optical for the wide companion. To classify the objects in a qualitative manner, we went through a direct visual comparison of the spectra with a set of known field dwarf spectral templates, separately in the optical and near-IR regimes. The optical spectra of known M dwarf templates were retrieved from the SDSS (York et al. 2000) spectroscopic data base provided by Bochanski et al. (2007). This data base contains a repository of good-quality composite spectra of low-mass dwarfs (M0–L0), one per subclass, spanning the 380–940 nm wavelength range. In the near-IR, we used the M dwarf spectral templates available in the IRTF Spectral Library,[2] which provides $R \sim 2000$ spectra with S/N $\gtrsim 100$ over the 0.8–2.5 μm range (Rayneretal 2009; Cushingetal 2005).

In Fig. 4, we display the optical and near-IR spectra (left-hand and right-hand panel, respectively) of NLTT 51469A overplotted with a grid of best-matching spectral templates. Regions contaminated by strong telluric absorption in the near-IR spectra around 1.4 and 1.9 μm were not considered in the comparison and are cleared for display. Also, the region at ∼1.15 μm (in the J band) appears to be affected by poor telluric correction. This may be due to the difference in airmass between the target and the standard star; none the less, this does not preclude the spectral type classification that makes use of the full spectral range. The M dwarfs used as comparison objects in the near-IR are HD 95735 (M2V), Gl 388 (M3V), and Gl 213 (M4V) (Cushing, Rayner & Vacca 2005; Rayner, Cushing & Vacca 2009). Fig. 5 contains a comparison of optical spectrum of the brown dwarf co-moving with NLTT 51469A with a grid of L8–T0 field dwarf spectra. The known objects used as templates are SDSS J085758.45+570851.4 (L8 ± 1), SDSS J083008.12+482847.4 (L9 ± 1), 2MASS J03284265+2302051 (L9.5 ± 0.5), and SDSS J042348.57−041403.5AB (T0 ± 0.5) and their data were taken from Golimowski et al. (2004), Knapp et al. (2004), and Chiu et al. (2006). The broad feature shortward of 1 micron in the spectrum of the object is due to lack of telluric correction.

For the primary, we determine a spectral type of M3.0 dwarf with a one subclass uncertainty, considering both optical and near-IR spectra. For the companion, we assign a spectral type of L9, with a one subclass uncertainty, using its optical spectrum. The M3 primary does not show strong molecular absorption due to CaH in the optical spectrum, thus indicating that this star is not a metal-depleted source, which contrasts with the results of the RAVE 4th data release catalogue (Kordopatis et al. 2013; [m/H] $= -2.31 \pm 0.18$). Indeed, as shown in Fig. 4, the optical spectrum of the primary is nicely reproduced by field, high-gravity solar-metallicity stars. The L9 ±1 type is consistent with the previous determination by Chiu et al. (2006), who classified the object using 0.8–2.5 μm near-IR spectra.

The optical/near-IR/mid-IR multiband colours of the primary: $V - I = 2.38 \pm 0.03$, $I - J = 1.35 \pm 0.05$, $J - K_s = 0.80 \pm 0.05$, $K_s - W1 = 0.15 \pm 0.05$ mag are compatible with the colours of M2–M4V spectral type standards (Kirkpatrick & McCarthy 1994; Pecaut & Mamajek 2013). The brown dwarf companion, with $z - J = 2.66 \pm 0.12$, $J - H = 0.81 \pm 0.03$, $J - K_s = 1.43 \pm 0.03$, and $J - W2 = 2.41 \pm 0.09$ mag, also shows an agreement with the typical colours of field-age late-L dwarfs; however, a large scatter of ∼0.5 mag and similarity of these colours of L5–T0 objects (Chiu et al. 2006; Dupuy & Liu 2012) prevent a more precise distinction of the spectral type from photometry.

5 BINARITY OF THE NLTT 51469 STAR

We have analysed the FastCam, Clio-2, and NACO images at the three epochs spanning a 1.9 yr baseline. Using imcentroid and adopting the instrument angle and pixel scale of FastCam at NOT of 30.5 ± 0.1 mas pixel^{-1} determined from astrometric calibrations using the M15 cluster images, we have measured a relative angular separation between the NLTT 51469A star and the additional nearby source of $\rho = 0.625 \pm 0.009$ arcsec and a position angle of $\theta = 57.28 \pm 0.76$ deg. From the Clio-2 observations, using pixel scale and orientation calibrations from Morzinski et al. (2015) we

[2] http://irtfweb.ifa.hawaii.edu/ spex/IRTF_Spectral_Library/

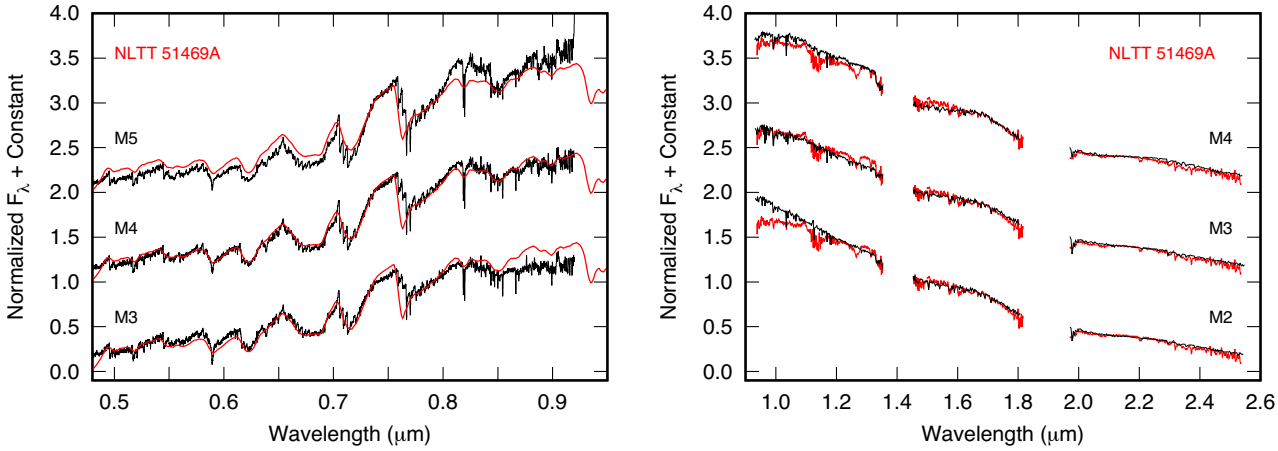

Figure 4. Low-resolution GTC/OSIRIS optical (left-hand panel) and NTT/SofI near-IR (right-hand panel) spectra of the primary NLTT 51469A plotted with red lines, compared to a grid of M2–M5 spectral templates with labels indicating their type. The sources and references of used templates are described in Section 4. Spectra were normalized at 0.9 μm at optical and at 1.65 μm at near-IR and offset by a constant for display.

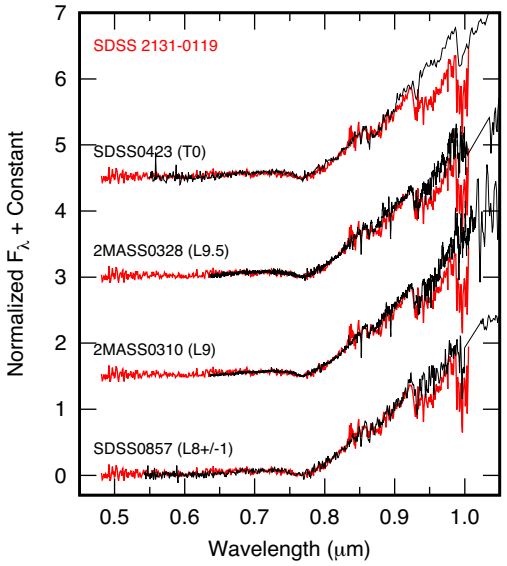

Figure 5. GTC/OSIRIS low-resolution optical spectrum of the brown dwarf companion SDSS 2131−0119 (red lines), overplotted with a set of spectra of known L8–T0 field dwarfs (black lines). Names and spectral types of used templates are labelled in the plot and corresponding references are given in Section 4. All spectra are normalized at 0.9 μm and shifted by a constant.

have measured ρ=0.6414 ± 0.0001 arcsec and θ=56.57 ± 0.13 deg and using our calibrations with 70 Oph, ρ=0.628 ± 0.012 arcsec and θ=56.59 ± 0.42 deg. From the NACO K_s-band image, we have measured ρ=0.638 ± 0.003 arcsec and θ=55.92 ± 0.13 deg with the instrument angle and 13.24 ± 0.04 mas pixel^{-1} pixel scale calibrated using the WDS 20204+0118 image in the same band. Considering the proper motion of the primary and the time span from FastCam observation, the ρ and θ would be 1.07 ± 0.02 arcsec and 41.6 ± 0.8 deg, respectively, if the secondary was a non-related background object.

From these images, we have also measured the relative flux between the two objects using the peak value ratio and psf photometry using the DAOPHOT package and determined the relative magnitude difference in each of the four bands. To account for the additional source, which is unresolved in 2MASS and DENIS, we deblended the catalogue magnitudes to give the appropriate values of individual components. The magnitudes, angular separations, and position angles are listed in Table 1.

Considering the relative high proper motion of the primary star of 260 mas yr^{-1}, and the expected magnitude of the secondary star of $I \sim$14.5 mag, the fainter component should have been detected at the same sky position in the old photographic plates of Digital Sky Survey images if it was a stationary background object. Having the three epoch images we prove that this close pair is indeed co-moving, as the measured angular separations and position angles remain consistent within 1.5σ. Moreover, the ρ and θ measured on the earliest and latest epoch observations differ by approximately 40σ and 20σ, respectively, from the values expected in case the secondary was a stationary object.

The probability that these two stars are found in such close proximity by chance is very low. Given the 0.6 arcsec separation and assuming a conservative distance range of 15–50 pc the space volume potentially occupied by the pair is $\lesssim$1.22 × 10^{-6} pc^3. Of all the *Gaia* DR2 stars within 100 pc and ±20 deg of NLTT 51469A, only 0.08 per cent share its proper motion at the 3σ level, considering a 5 mas yr^{-1} error in the proper motion of the M3. Coupling this with the local space density of 0.06–0.11 stars pc^{-3} (Reid, Cruz & Allen 2007), we estimate that the probability of a chance alignment in space and motion for these two objects is less than 1.1 × 10^{-10}. We can thus conclude that both stellar components are physically bound.

Using the absolute magnitude-spectral type and colour-spectral type relations from Pecaut & Mamajek (2013), and the spectral type determination of the primary, we estimate that the secondary is an M6 ± 1 dwarf from the derived relative magnitude differences in the four bands and the photometric colours: $I - J = 2.31 \pm 0.33$, $I - K_s = 3.04 \pm 0.32$, $J - K_s = 0.73 \pm 0.05$.

6 DISTANCE

The *Gaia* DR2 provided the parallax measurement for the primary NLTT 51469, $\pi = 21.457 \pm 0.611$ mas, which translates to a distance of 46.6 ± 1.3 pc. The object at 0.″64 from the primary was not resolved by *Gaia*; however, NLTT 51469 was tagged as a duplicated source in the DR2 catalogue. The brown dwarf companion SDSS 2131−0119 was beyond the detection limit of

Table 1. Photometry and astrometry of NLTT 51469AB.

Instr., band	mag(A)	mag(B)	ρ (arcsec)	θ (deg)	Epoch (MJD)
FastCam *I*	11.25 ± 0.30	14.55 ± 0.30	0.625 ± 0.009	57.28 ± 0.76	57708
Clio-2 *J*	9.98 ± 0.06	12.21 ± 0.06	0.628 ± 0.012	56.59 ± 0.42	58240
NACO *J*	9.975 ± 0.031	12.245 ± 0.031	0.641 ± 0.003[a]	55.95 ± 0.16[a]	58415
NACO *H*	9.399 ± 0.023	11.751 ± 0.023	0.638 ± 0.003[a]	56.15 ± 0.14[a]	58415
NACO K_s	9.163 ± 0.025	11.513 ± 0.025	0.638 ± 0.003	55.92 ± 0.13	58415

Note: [a] Using pixel scale and orientation calibration from Köhler et al. (2016).

Table 2. Spectrophotometric distance estimates for SDSS 2131−0119.

Method	Ref.	*d* (pc)	Δ/σ
M_J versus SpT	F15	38 (+7, −11)	0.94
M_H versus SpT	F15	39 (+7, −11)	0.83
M_{Ks} versus SpT	F15	41 (+6, −12)	0.61
M_{W1} versus SpT	F15	40 (+14, −11)	0.52
M_{W2} versus SpT	F15	46 (+14, −11)	0.05
M_J versus SpT	D12	33 (+12, −8)	1.34
M_{W2} versus SpT	D12	44 (+15, −11)	0.20
Mean		40.1 ± 10.7	0.64

Note: References. – (F15): Filippazzo et al. (2015); (D12): Dupuy & Liu (2012).

Gaia. To assess whether it is located at a consistent distance, we have estimated its spectrophotometric distance, assuming that the system has the age of the field. We used the VHS *J*, *H*, K_s and *WISE W*1 and *W*2 photometry with near- and mid-infrared absolute magnitude versus spectral type relations for field L and T dwarfs defined in Dupuy & Liu (2012) and Filippazzo et al. (2015). In Table 2, we list the obtained estimates and their uncertainties, which take into account uncertainties in spectral type determination, intrinsic scatter of absolute magnitudes of a given spectral type, and errors in photometry. The Δ/σ ratios quantify the difference between the parallactic distance of the primary and the estimated spectrophotometric distance of the L9 relative to the corresponding uncertainties. The values are consistent within the errors for all the considered bands and yield a mean distance of the L9 of 40 ± 11 pc. This distance constraint for the L9 is consistent with the parallactic distance of NLTT 51469 at a level of 1σ.

We estimated the spectrophotometric distance also for the primary, for which we employed the DENIS *I* and 2MASS *J*, *H*, K_s photometry, since at these magnitudes the VHS starts to get beyond the linear regime of the detector. To account for the source at 0.″64 being unresolved in DENIS and 2MASS, we use the deblended magnitudes and by considering the mean absolute magnitudes for a given early-mid M subtype from the compilation of Pecaut & Mamajek (2013) we find $d_I = 33 \pm 17$ pc and $d_{JHK_s} = 34^{+10}_{-13}$ pc. The large errors are mainly due to uncertainty in spectral type, since a range from M2 to M4 implies an ∼1.5 mag difference in brightness in these bands. The spectrophotometric distance of the primary is slightly lower but consistent with the parallactic distance to within the 2σ uncertainty level. The spectrophotometric distance values of both objects also coincide, reinforcing that they are located at the same distance, which is consistent with companionship.

In our further analysis, we consider both the *Gaia* distance to the system, i.e. 46.6 ± 1.3 pc, and the spectrophotometric distance of 34^{+10}_{-13} pc. The corresponding projected orbital separations between the components are ∼2800–3800 au (M3 and L9) and 22–30 au (M3 and ∼M6). For these two distances, we compare the absolute *J* magnitudes versus $J - K_s$ colours of the M3, ∼M6, and L9

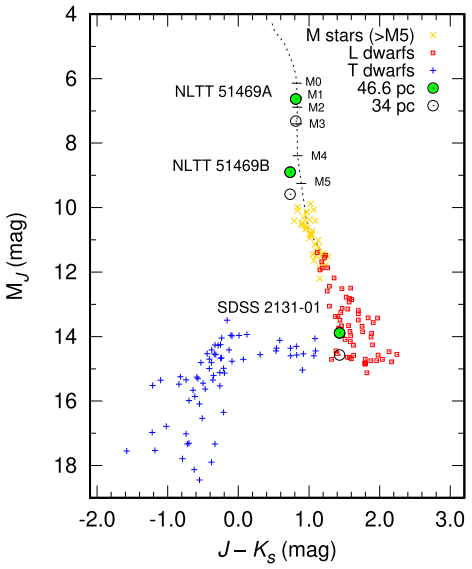

Figure 6. M_J versus $J - K$ colour–magnitude diagram showing the two components of the NLTT 51469AB binary star and its wide L9 ± 1 brown dwarf companion overplotted against the sequence of K and M stars (Pecaut & Mamajek 2013) and ultracool dwarfs with measured parallactic distances from Dupuy & Liu (2012). For the system, we consider both the *Gaia* DR2 distance of $d = 46.6 \pm 1.3$ pc and our spectrophotometric estimation at $d \sim$ 34 pc.

components on the colour–magnitude diagram in Fig. 6 with a sequence of K and M stars (Pecaut & Mamajek 2013) and field late-M, L, and T dwarfs with measured parallaxes compiled in Dupuy & Liu (2012).

The components follow the sequence and have photometric colours in agreement with those expected for their spectral type, but, adopting the 46.6 pc distance all the three objects appear about 1 mag brighter than their standard counterparts of the corresponding spectral type. The primary matches better to an M1–M2 and the secondary to an M4–M5-type dwarf. We suggest that this may be due to parallax determination being affected by the companion at 0.″64 unresolved by *Gaia*.

Evidence has been reported in other similar cases (e.g. 2MASS J0249−0557AB, Dupuy et al. 2018) that the five-parameter *Gaia* DR2 astrometric solutions can be altered, in a systematic way, by the orbital motion of unresolved binaries. Particularly when a relatively small number of independent observation epoch was available (DR2 reports that only eight visibility periods were used in case of NLTT 51469). The astrometric excess noise of the source in DR2 is $\epsilon_i = 2.74$ mas at a significance of 2202σ, indicating that indeed the *Gaia* astrometry of this binary is most likely affected by correlated noise from orbital motion. The parallax is 15σ lower than it would be expected from the spectrophotometric distance,

but, as noted by Dupuy et al. 2018, DR2 parallax systematics for unresolved binaries can be up to $\approx 20\sigma$. The forthcoming *Gaia* data release with improved astrometry of non-single stars and with the binary information reported in our paper shall provide a more accurate distance for the system.

7 COMPANIONSHIP OF NLTT 51469AB AND SDSS 2131−01

To evaluate whether the NLTT 51469 and SDSS 2131−01 objects are physically bound or if they have been found together at this separation due to chance alignment, we estimated the probability of finding an L, T-type dwarf in our common proper motion search for companions and that both objects have consistent proper motion within 50 mas yr^{-1}.

To calculate the contamination rate of L, T dwarfs, we need to determine the density of such objects in the VHS survey down to the limiting magnitude of 2MASS. To do this, we have found that about 400 L and Ts are identified in the full VHS area (∼20 000 deg^2), implying a surface density of 0.02 objects per square degree, and hence the probability for the presence of an L or T dwarf up to 20 arcmin around a star is 0.67 per cent. To estimate the probability that the companion is not physically related but has a consistent proper motion with the primary, we have identified that 548 objects out of 50 382 in our HPM catalogue have common proper motion with NLTT 51469, which represents a probability of 1.1 per cent.

Assuming a poissonian distribution, the probability of finding an L or T dwarf whose proper motion is consistent with a nearby NLTT star in our VHS search is given by

$$P_{(x>0)} = 1 - P_{(x=0)} = 1 - \mathrm{e}^{-\lambda}, \text{ where } \lambda = np, \quad (1)$$

where P is the poissonian probability distribution, n the number of stars, and p the combined probability of finding LT dwarfs with consistent proper motion. For our search, we estimate that this probability is 26 per cent (it is relatively low, but not negligible). Considering that SDSS 2131−01 was found at an angular separation of 82.3 arcsec, the probability to find such objects within this separation is much lower (0.14 per cent). In this calculation, we have not taken into account that additionally, both objects appear to be located at a consistent distance. In summary we conclude that it is highly unlikely that the two components are unrelated objects found by chance alignment, and therefore that the NLTT 51469AB and SDSS 2131−01 are a physically bound multiple system.

8 PHYSICAL PROPERTIES

8.1 Radial velocity, galactic kinematics, and age

We employed the LT/FRODOSpec intermediate-resolution red optical spectrum ($R \sim 5000$, 600–800 nm) of NLTT 51469A, displayed in Fig. 7, to measure its heliocentric radial velocity, at the mean Modified Julian Date, MJD = 57593.061387. We used the cross-correlation method against the M4.5V star GJ 876, which has a known, constant radial velocity of $v_\mathrm{h} = 0.413 \pm 0.124$ km s^{-1} (Nidever et al. 2002). The cross-correlation was computed using the FXCOR task within IRAF over 6500–7500 and 7700–7950 Å wavelength range containing good signal-to-noise (S/N > 50) data not affected by the telluric absorption. We fit a Gaussian function to the peak of the cross-correlation distribution. The resulting relative displacement was corrected for the lunar, diurnal, and annual velocities to obtain the heliocentric radial velocity of NLTT 51469A. We measured $v_\mathrm{h} = -64.3 \pm 9.0$ km s^{-1}, where the error bar

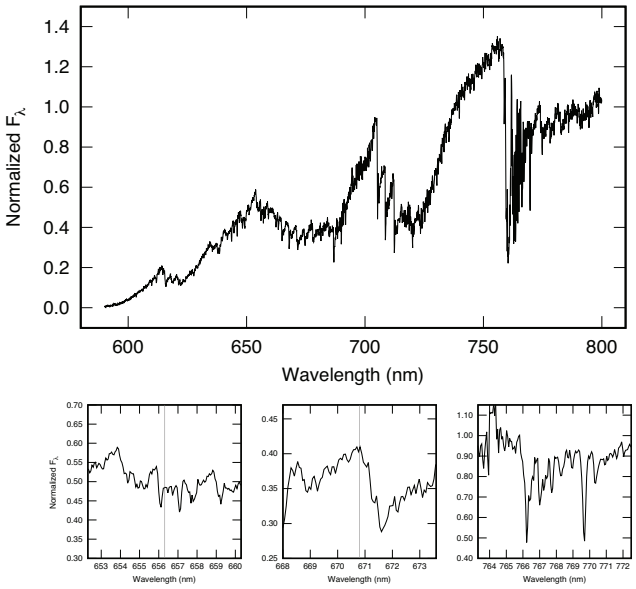

Figure 7. LT/FRODOSpec spectrum of NLTT 51469A covering a 580–900 nm wavelength range at a resolution of $R \sim 5300$. No telluric correction or flux calibration was applied to the displayed spectrum. The bottom plots show a close-up of λ regions of Hα, Li I, and K I doublet lines.

accounts for the uncertainties due to the cross-correlation procedure and the error associated with the velocity of the M4.5V standard star.

The star has a previous radial velocity measurement obtained by Kordopatis et al. (2013) on 2009 October 17 (MJD = 55121), ∼7 yr before our FRODOSpec observation. These authors obtained $v_\mathrm{h} = -67.34 \pm 2.76$ km s^{-1}, which is consistent with our determination within the error bars. *Gaia* DR2 does not provide the radial velocity of the M3 primary, but it does provide $T_\mathrm{eff} = 3654$ K. The ∼M6-type companion at 0.″64 induces a radial velocity variation of a maximum semi-amplitude of about 1 km s^{-1} over an orbital period of roughly 200 yr for an edge-on, circular orbit. This implies a shift of up to ∼10 m s^{-1} per year for an edge-on orbit, readily measurable with modern spectrographs.

Having the proper motion, radial velocity, and parallactic distance, we calculated the three components of the Galactic space velocity, U, V, and W of NLTT 51469A applying the formulas given by Johnson & Soderblom (1987). We used the more precise literature value of v_h for the calculation, and derived U, V, $W = 8.0 \pm 1.8$, -82.4 ± 2.1, 30.3 ± 1.7 km s^{-1}, respectively. The errors take into account the uncertainties of the proper motion, distance, and radial velocity. Fig. 8 illustrates the ellipsoids corresponding to well-characterized young stellar moving groups of the solar neighbourhood (data compiled from Zuckerman & Song 2004 and Torres et al. 2008) and the space velocity of NLTT 51469. The high V and W indicate that the star does not belong to any of the nearby young moving groups; its velocities are compatible with velocity dispersions of the thin galactic disc population (Leggett 1992, and references therein).

We also used the FRODOSpec spectrum to look for spectral features recognized as indicators of youth in very low-mass stars. We investigate the lithium content (Li I line at 670.8 nm), the H$_\alpha$ emission line at 656.3 nm, and the potassium doublet at 766.5 and 769.9 nm. We did not detect the Li I absorption line with detection upper limit on the pseudo-equivalent width (pEW) of 60 mÅ nor

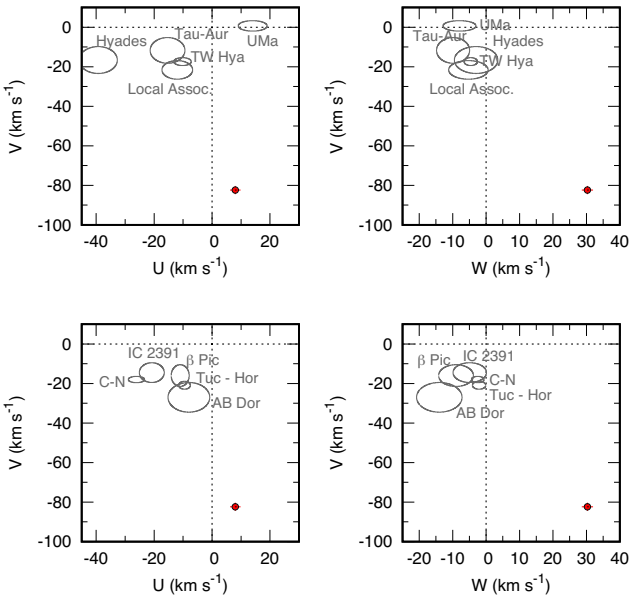

Figure 8. Galactic space velocities of NLTT 51469 (red dots) with overplotted ellipsoids of known young star associations and moving groups. Errors incorporate uncertainties in the proper motion, parallactic distance, and radial velocity. Galactocentric U velocity is positive towards the Galactic centre.

H_α emission at the level higher than -0.5 Å. For the K I lines, we measure pEWs of 1.0 ± 0.2 and 1.1 ± 0.1 Å.

No significant H_α emission suggests low chromospheric activity, indicative of a spun-down M dwarf. The absence of lithium and the relatively high V and W galactic velocities rule out youth. Also, the non-detection in X-rays by the *ROSAT* All Sky Survey and the GALEX UV detection with NUV $= 23.05 \pm 0.30$ mag (2.2 ± 0.6 μJy) and non-detection in FUV indicate no significant flux excess, as compared to early M dwarfs at young ages until a few hundred Myr, and agree with ages older than the Hyades at 650 Myr, for which a decay in UV and X-ray flux excess reaches a factor of 20 and 65 (Stelzer et al. 2013; Shkolnik & Barman 2014). Together, these criteria point to the NLTT 51469 system belonging to the thin disc population, with a likely age in the range of ∼1–5 Gyr.

8.2 Luminosity, mass, and effective temperature

We determined the bolometric magnitude and luminosity of the primary using JHK_s-band photometry from 2MASS, decomposed to account for an additional, unresolved ∼M6 source, and the bolometric corrections (BCs) for field M dwarfs from table 5 in Pecaut & Mamajek (2013). We employed the solar bolometric magnitude of 4.74 mag and obtained $M_{\rm bol} = 8.48^{+0.10}_{-0.05}$ mag and a luminosity of $\log(L_{\rm bol}/L_\odot) = -1.50^{+0.02}_{-0.04}$ dex. Errors in this determination include error in distance (parallax), spectral type, and photometry. These values correspond to a rather earlier type at around M1.5, whereas for an M3 ± 1 dwarf one would expect $M_{\rm bol} \sim 9.2^{+1.0}_{-0.5}$ mag and a luminosity of $-1.78^{+0.2}_{-0.4}$ dex. As mentioned earlier, this discrepancy may be a result of an error in the parallax determination due to the stellar companion at 0.6 arcsec.

For the estimation of effective temperature and mass, we also used the values from the compilation of Pecaut & Mamajek (2013), which for an M3 ± 1 dwarf yield a $T_{\rm eff} = 3410^{+140}_{-210}$ K and $m = 0.36^{+0.08}_{-0.14}$ $M_\odot$. The *Gaia* parallactic distance implies a higher luminosity than expected for an M3 dwarf and hence mass estimate based on the mass–luminosity relation for main-sequence M dwarfs (Benedict et al. 2016) yields a consequently higher range of $m = 0.42 \pm 0.02$ $M_\odot$. As for the ∼M6 component, based on the values from Pecaut & Mamajek (2013) as reference values for a

Table 3. Measurements and determined parameters of the system.

Astrometry	NLTT 51469	SDSS 2131−0119
R.A. (J2000)	$21^h31^m59^s.603$	$21^h31^m54^s.391$
Decl. (J2000)	$-01°20'06''.554$	$-01°19'40''.511$
2MASS ID	J213159.66−012003.9	J213154.44−011937.4
Separation (arcsec)[a]	82.27 ± 0.02	
Separation (au)	3834 ± 100	
Position angle (deg)[a]	288.4 ± 0.1	
$\mu_\alpha \cos\delta$ (mas yr^{-1})	-106 ± 5	-100 ± 20
μ_δ (mas yr^{-1})	-235 ± 5	-230 ± 20
$\mu_\alpha \cos\delta$ (mas yr^{-1})[b]	-95.49 ± 0.96	–
μ_δ (mas yr^{-1})[b]	-239.38 ± 0.96	–
Parallax π (mas)[b]	21.45 ± 0.61	–
Estimated d (pc)	34^{+10}_{-13}	40 ± 11
Parallactic d (pc)	46.6 ± 1.3	–
v_r (km s^{-1})[c]	-67.34 ± 2.76	–
	-64.3 ± 9.0	–
U (km s^{-1})	7.12 ± 1.61	–
V (km s^{-1})	-82.56 ± 2.12	–
W (km s^{-1})	30.16 ± 1.80	–
Photometry (mag)		
V	13.58 ± 0.01	–
R	13.47 ± 0.09	–
I	11.20 ± 0.02	–
G	12.677 ± 0.001	–
Sloan g	15.604 ± 0.006	–
Sloan r	13.369 ± 0.001	–
Sloan i	12.040 ± 0.001	>22.68
Sloan z	13.116 ± 0.013	19.890 ± 0.100
2MASS J	9.848 ± 0.029	17.396 ± 0.263
2MASS H	9.281 ± 0.021	15.781 ± 0.194
2MASS K_s	9.045 ± 0.023	15.559 ± 0.210
VHS J	<10.88	17.230 ± 0.015
VHS H	<11.10	16.419 ± 0.016
VHS K_s	<10.10	15.796 ± 0.018
*WISE W*1	8.894 ± 0.022	15.075 ± 0.037
*WISE W*2	8.736 ± 0.019	14.824 ± 0.072
*WISE W*3	8.610 ± 0.028	–
*WISE W*4	8.123 ± 0.294	–
Spectral classification		
Optical	$M3.5 \pm 0.5$	$L9.0 \pm 1.0$
Near-IR	$M3.0 \pm 1.0$	$L9.0 \pm 0.5$[d]
Adopted spectral type	$M3.0 \pm 1.0$	$L9.0 \pm 1.0$
Physical Properties		
Age (Gyr)	1–10	
$\log(L_{\rm bol}/L_\odot)$	$-1.50^{+0.02}_{-0.04}$	-4.4 ± 0.1
$\log(L_{\rm bol}/L_\odot)$[e]	$-1.78^{+0.02}_{-0.04}$	$-4.7^{+0.3}_{-0.5}$
$T_{\rm eff}$ (K)	3410^{+140}_{-210}	1400–1650
Mass ($M_\odot$)	0.42 ± 0.02	0.05–0.07

Note: [a]Measured using VHS images, epoch (MJD) = 55373.363111.
[b]From the *Gaia* DR2.
[c]Literature value and our measurement.
[d]Near-IR spectral type from Chiu et al. (2006).
[e]Considering spectrophotometric distance.

given spectral type we estimated $T_{\rm eff}$ and mass of 2850 ± 200 K and $0.10^{+0.06}_{-0.01}$ $M_\odot$, respectively.

For the L9 companion, we determined the bolometric magnitude and luminosity using the BC for field-age ultracool dwarfs from Filippazzo et al. (2015) and *J*-band photometry from VHS. Considering $d = 46.6 \pm 1.3$ pc, we obtained $M_{\rm bol} = 15.71 \pm 0.25$ mag and $\log(L_{\rm bol}/L_\odot) = -4.4 \pm 0.1$ dex, whereas for $d = 34^{+10}_{-13}$ pc we got $16.40^{+1.17}_{-0.69}$ mag and $-4.66^{+0.28}_{-0.47}$ dex, taking into account errors in distance, spectral type, photometry, and intrinsic scatter of absolute magnitudes at a given spectral type. We then employed the AMES Dusty evolutionary model isochrones (Allard et al. 2001; Allard, Homeier & Freytag 2011, 2012) to infer the $T_{\rm eff}$ and mass of the companion for three different ages and solar abundance, using the *Gaia* distance. We obtained masses between 0.050–0.055, 0.068–0.071, and 0.068–0.071 $M_\odot$ and temperatures in the range of 1400–1550, 1450–1600, and 1500–1650 K for 1, 5, and 10 Gyr, respectively. The obtained values are compiled in Table 3. From the polynomial relations of $L_{\rm bol}$ and $T_{\rm eff}$ as a function of spectral type for field-age objects determined by Filippazzo et al. (2015), the expected luminosity and temperature of an L9-type object are -4.55 ± 0.13 dex and 1300 ± 120 K, respectively. These values are somewhat lower than the ones derived using BCs, *J*-band photometry, and parallactic distance, but consistent within the errors.

9 CONCLUSIONS AND FUTURE PROSPECTS

Using the VHS and 2MASS surveys and follow-up imaging and spectroscopic observations, we have identified a very low mass hierarchical triple system, NLTT 51469AB/SDSS 2131−0119, composed of a close stellar binary at an angular separation of 0.64 ± 0.01 arcsec (projected distance of ≈ 30 au), and a wide (82.27 ± 0.02 arcsec, ≈ 3800 au) co-moving brown dwarf companion. We determined the spectral type of the primary NLTT 51469A and confirm the spectral type of the brown dwarf as M3 ± 1 and L9 ± 1, respectively. We have also estimated the spectral type of the close companion NLTT 51469B to be ∼M6 ± 1.

The *Gaia* measurement of the parallax of NLTT 51469 yields a distance of 46.6 ± 1.3 pc. Our spectrophotometric distance estimates are compatible with this, though indicate the possibility of a slightly closer distance (that may be consistent with *Gaia* uncertainty induced by multiplicity). The matching proper motions and agreement in distance of the M3 and L9 components, and the compatible angular separations and position angles of the ∼M6 component measured at three epochs lead us to the conclusion that the three objects form a physically bound system.

We determined the luminosities, effective temperatures, and masses of the three components. It is worth noting that an age near 1 Gyr (at the younger end of the thin disc range) would imply a mass of the L9 brown dwarf at or below 0.055 $M_\odot$, and thus preservation of lithium (Magazzu, Martin & Rebolo 1993). Intermediate-resolution spectroscopy covering the Li I line at 670.8 nm could thus be useful in providing additional age constraints.

Assuming masses of 0.4 $M_\odot$ for the M3, 0.1 $M_\odot$ for the M6, and 0.065 $M_\odot$ for the L9, and given the ∼3800 au separation of the L9 companion, this is certainly one of the systems with the lowest gravitational binding energy ($E_{\rm b} \approx -2.48 \times 10^{42}$ erg). Yet, it can be energetically stable according to fig. 16 of Close et al. (2007). This might be telling us that the system was not formed in a dense environment, otherwise, encounters with other stars would have disrupted the least massive component. Another possibility is that the system we see today is the result of capture(s) from gravitational interactions with nearby or passing low-mass sources. Only by characterizing the long- and short-period orbits and performing an exhaustive analysis of the chemical composition of each individual member of the system, we might be able to assess their origin. The presented system builds up the sample of benchmark objects for studies of the least massive stars and substellar objects, in particular, of brown dwarfs at the L/T transition.

ACKNOWLEDGEMENTS

We sincerely thank the reviewer for his insightful comments that allowed us to greatly improve the manuscript.

BG acknowledges support from the CONICYT through FONDECYT Postdoctoral Fellowship grant no. 3170513. This work is partly financed by the Spanish Ministry of Economy and Competitiveness through the project AYA2016-79425-C3-2-P. NL and VJSB acknowledge support from the Spanish Ministry of Economy and Competitivity through the project AYA2015-69350-C3-2-P. AP acknowledges support from the Spanish Ministry of Economy and Competitivity through the project AYA2015-69350-C3-3-P. Based on observations obtained as part of the VHS, ESO programme, 179.A-2010 (PI: McMahon). Based on observations collected at the European Organisation for Astronomical Research in the Southern hemisphere under ESO programme 092.C-0874(B). Based on observations made with the NOT, operated by the Nordic Optical Telescope Scientific Association at the Observatorio del Roque de los Muchachos, La Palma, Spain, of the Instituto de Astrofísica de Canarias. This paper includes data obtained using the 6.5 m Magellan Clay Telescope at Las Campanas Observatory, Chile. This publication makes use of data products from the Two Micron All Sky Survey, which is a joint project of the University of Massachusetts and the Infrared Processing and Analysis Center/California Institute of Technology, funded by the National Aeronautics and Space Administration and the National Science Foundation. This publication makes use of data products from the Wide-field Infrared Survey Explorer, which is a joint project of the University of California, Los Angeles, and the Jet Propulsion Laboratory/California Institute of Technology, funded by the National Aeronautics and Space Administration. This work has made use of data from the European Space Agency (ESA) mission *Gaia* (https://www.cosmos.esa.int/gaia), processed by the *Gaia* Data Processing and Analysis Consortium (DPAC, https://www.cosmos.esa.int/web/gaia/dpac/consortium). Funding for the DPAC has been provided by national institutions, in particular the institutions participating in the *Gaia* Multilateral Agreement. This research has made use of NASA's Astrophysics Data System. We have made use of the *ROSAT* Data Archive of the Max-Planck-Institut für extraterrestrische Physik (MPE) at Garching, Germany. This research has made use of the Washington Double Star Catalog maintained at the U.S. Naval Observatory.

REFERENCES

Abazajian K. et al., 2003, AJ, 126, 2081
Ackerman A. S., Marley M. S., 2001, ApJ, 556, 872
Allard F., Hauschildt P. H., Alexander D. R., Starrfield S., 1997, ARA&A, 35, 137
Allard F., Hauschildt P. H., Alexander D. R., Tamanai A., Schweitzer A., 2001, ApJ, 556, 357
Allard F., Homeier D., Freytag B., 2011, in Johns-Krull C., Browning M. K., West A. A., eds, ASP Conf. Ser. Vol. 448, 16th Cambridge Workshop

on Cool Stars, Stellar Systems, and the Sun. Astron. Soc. Pac., San Francisco, p. 91
Allard F., Homeier D., Freytag B., 2012, Phil. Trans. R. Soc. London Ser. A, 370, 2765
Barnsley R. M., Smith R. J., Steele I. A., 2012, Astron. Nachr., 333, 101
Baron F. et al., 2015, ApJ, 802, 37
Benedict G. F. et al., 2016, AJ, 152, 141
Bochanski J. J., West A. A., Hawley S. L., Covey K. R., 2007, AJ, 133, 531
Burgasser A. J., Burrows A., Kirkpatrick J. D., 2006b, ApJ, 639, 1095
Burgasser A. J., Geballe T. R., Leggett S. K., Kirkpatrick J. D., Golimowski D. A., 2006a, ApJ, 637, 1067
Burningham B. et al., 2008, MNRAS, 391, 320
Burrows A., Sudarsky D., Hubeny I., 2006, ApJ, 640, 1063
Cepa J., 2010, in Diego J. M., Goicoechea L. J., González-Serrano J. I., Gorgas J., eds, Highlights of Spanish Astrophysics V. Springer-Verlag, Berlin, p. 15
Chabrier G., Baraffe I., Allard F., Hauschildt P., 2000, ApJ, 542, 464
Chiu K., Fan X., Leggett S. K., Golimowski D. A., Zheng W., Geballe T. R., Schneider D. P., Brinkmann J., 2006, AJ, 131, 2722
Close L. M. et al., 2007, ApJ, 660, 1492
Cushing M. C., 2005, ApJ, 623, 1115
Cushing M. C., Rayner J. T., Vacca W. D., 2005, ApJ, 623, 1115
Cushing M. C. et al., 2011, ApJ, 743, 50
Deacon N. R. et al., 2014, ApJ, 792, 119
Delfosse X. et al., 1997, A&A, 327, L25
Dupuy T. J., Liu M. C., 2012, ApJS, 201, 19
Dupuy T. J. et al., 2018, AJ, 156, 57
Emerson J. P., Sutherland W. J., McPherson A. M., Craig S. C., Dalton G. B., Ward A. K., 2004, The Messenger, 117, 27
Epchtein N. et al., 1994, Ap&SS, 217, 3
Faherty J. K., Burgasser A. J., West A. A., Bochanski J. J., Cruz K. L., Shara M. M., Walter F. M., 2010, AJ, 139, 176
Filippazzo J. C., Rice E. L., Faherty J., Cruz K. L., Van Gordon M. M., Looper D. L., 2015, ApJ, 810, 158
Filippenko A., Greenstein J. L., 1984, PASP, 96, 530
Gaia Collaboration, 2016, A&A, 595, A1
Gaia Collaboration, 2018, A&A, 616, A1
Golimowski D. A. et al., 2004, AJ, 127, 3516
Gomes J. I. et al., 2013, MNRAS, 431, 2745
Gould A., Salim S., 2003, ApJ, 582, 1001
Jenkins J. S. et al., 2012, MNRAS, 420, 3587
Johnson D. R. H., Soderblom D. R., 1987, AJ, 93, 864
Kaiser N. et al., 2002, in Tyson J. A., Wolff S., eds, Proc. SPIE Conf. Ser. Vol. 4836, Survey and Other Telescope Technologies and Discoveries. SPIE, Bellingham, p. 154
Kirkpatrick J. D., 2005, ARA&A, 43, 195
Kirkpatrick J. D., McCarthy D. W., Jr, 1994, AJ, 107, 333
Kirkpatrick J. D. et al., 1999, ApJ, 519, 802
Kirkpatrick J. D. et al., 2011, ApJS, 197, 19
Kirkpatrick J. D. et al., 2012, ApJ, 753, 156
Knapp G. R. et al., 2004, AJ, 127, 3553
Kordopatis G. et al., 2013, AJ, 146, 134
Köhler R., Kasper M., Herbst T. M., Ratzka T., Bertrang G. H.-M., 2016, A&A, 587, A35
Labadie L. et al., 2011, A&A, 526, A144
Lawrence A. et al., 2007, MNRAS, 379, 1599
Leggett S. K., 1992, ApJS, 82, 351
Leggett S. K., Tremblin P., Esplin T. L., Luhman K. L., Morley C. V., 2017, ApJ, 842, 118
Leggett S. K. et al., 2009, ApJ, 695, 1517
Lenzen R., Hofmann R., Bizenberger P., Tusche A., 1998, in Fowler A. M., ed., Proc. SPIE Conf. Ser. Vol. 3354, Infrared Astronomical Instrumentation. SPIE, Bellingham, p. 606
Luhman K. L., 2014, ApJ, 786, L18
Magazzu A., Martin E. L., Rebolo R., 1993, ApJ, 404, L17
Marocco F. et al., 2017, MNRAS, 470, 4885
Masciadri E., Brandner W., Bouy H., Lenzen R., Lagrange A. M., Lacombe F., 2003, A&A, 411, 157
Mason B. D., Wycoff G. L., Hartkopf W. I., Douglass G. G., Worley C. E., 2001, AJ, 122, 3466
McMahon R. G., Banerji M., Gonzalez E., Koposov S. E., Bejar V. J., Lodieu N., Rebolo R., VHS Collaboration, 2013, The Messenger, 154, 35
Morales-Rueda L., Carter D., Steele I. A., Charles P. A., Worswick S., 2004, Astron. Nachr., 325, 215
Morzinski K. M. et al., 2015, ApJ, 815, 108
Nakajima T., Oppenheimer B. R., Kulkarni S. R., Golimowski D. A., Matthews K., Durrance S. T., 1995, Nature, 378, 463
Nidever D. L., Marcy G. W., Butler R. P., Fischer D. A., Vogt S. S., 2002, ApJS, 141, 503
Oke J. B., 1990, AJ, 99, 1621
Oscoz A. et al., 2008, in Ian S. M., Mark M. C., eds, Proc. SPIE Conf. Ser. Vol. 7014, Ground-based and Airborne Instrumentation for Astronomy II. SPIE, Bellingham, p. 701447
Pecaut M. J., Mamajek E. E., 2013, ApJS, 208, 9
Pinfield D. J., Jones H. R. A., Lucas P. W., Kendall T. R., Folkes S. L., Day-Jones A. C., Chappelle R. J., Steele I. A., 2006, MNRAS, 368, 1281
Pourbaix D., 2000, A&AS, 145, 215
Rayner J. T., 2009, ApJS, 185, 289
Rayner J. T., Cushing M. C., Vacca W. D., 2009, ApJS, 185, 289
Rebolo R., Zapatero Osorio M. R., Martín E. L., 1995, Nature, 377, 129
Reid I. N., Cruz K. L., Allen P. R., 2007, AJ, 133, 2825
Robert J. et al., 2016, ApJ, 830, 144
Rousset G. et al., 2003, in Wizinowich P. L., Bonaccini D., eds, Proc. SPIE Conf. Ser. Vol. 4839, Adaptive Optical System Technologies II. SPIE, Bellingham, p. 140
Salim S., Gould A., 2003, ApJ, 582, 1011
Saumon D., Marley M. S., 2008, ApJ, 689, 1327
Scholz R.-D., 2016, A&A, 587, A51
Scholz R.-D., Bihain G., Schnurr O., Storm J., 2012, A&A, 541, A163
Shkolnik E. L., Barman T. S., 2014, AJ, 148, 64
Skrutskie M. F. et al., 2006, AJ, 131, 1163
Smart R. L., Marocco F., Caballero J. A., Jones H. R. A., Barrado D., Beamín J. C., Pinfield D. J., Sarro L. M., 2017, MNRAS, 469, 401
Steele I. A. et al., 2004, in Oschmann J. M., Jr, ed., Proc. SPIE Conf. Ser. Vol. 5489, Ground-based Telescopes. SPIE, Bellingham, p. 679
Stelzer B., Marino A., Micela G., López-Santiago J., Liefke C., 2013, MNRAS, 431, 2063
Torres C. A. O., Quast G. R., Melo C. H. F., Sterzik M. F., 2008, in Reipurth B., ed., Young Nearby Loose Associations, ASP, San Francisco, CA, p. 757
van der Marel R. P., Gerssen J., Guhathakurta P., Peterson R. C., Gebhardt K., 2002, AJ, 124, 3255
van Leeuwen F., 2007, A&A, 474, 653
Velasco S. et al., 2016, MNRAS, 460, 3519
Wright E. L. et al., 2010, AJ, 140, 1868
York D. G. et al., 2000, AJ, 120, 1579
Zapatero Osorio M. R., Béjar V. J. S., Miles-Páez P. A., Peña Ramírez K., Rebolo R., Pallé E., 2014, A&A, 568, A6
Zuckerman B., Song I., 2004, ARA&A, 42, 685

This paper has been typeset from a TEX/LATEX file prepared by the author.